Bartek Wierzba*, Jolanta Romanowska, Maryana Zagula-Yavorska, Janusz Markowski and Jan Sieniawski

# The Ni-Al-Zr Multiphase Diffusion Simulations

**Abstract:** The generalized Darken method allows a quantitative description of diffusion mass transport in multiphase materials. The method characterizes the diffusion zone by phase volume fractions. The results of the calculations are compared with experimental concentration's profiles of nickel, zirconium and aluminum in zirconium doped aluminide coatings deposited on pure nickel by the PVD and CVD methods.

**Keywords:** NiAlZr system, reactive diffusion, simulation, Zr content

**PACS® (2010).** 81.15.Gh, 07.05.Tp

DOI 10.1515/htmp-2014-0080
Received May 14, 2014; accepted August 19, 2014;
published online October 31, 2014

## 1 Introduction

The aluminizing process is extensively used to form protective coatings on aircraft turbine blades made of superalloys [1–11]. Aluminizing process is realized in many ways, such as: pack cementation, above-the-pack or physical and chemical vapor deposition methods. Chemical vapor deposition method has several advantages in comparison to the above-the-pack process. It allows deposition of the aluminide coatings on the internal cooling canals of the turbine blades, and control of the batch cooling rate. It provides heat treatment of the alloys that reduces cost of the process. Aluminide coatings deposited on nickel-based superalloys by the CVD method provide a good oxidation and corrosion resistance of blades. Addition of small amounts of reactive elements such as Zr, Hf, Y, or Ce to the NiAl coatings has beneficial effects on the oxidation behavior. The beneficial effects include improvement in adhesion of alumina scales and reduction of oxide scale growth rate [12, 13]. Zirconium co-deposited with aluminum on the nickel superalloy by the CVD process was developed by ONERA and SNECMA [14]. Zirconium provided by the $ZrOCl_2$-$8H_2O$ activator [14] locates far below the coating surface, at the interface between the β-NiAl coating and the interdiffusion zone. During oxidation zirconium migrates towards the surface and the Zr distribution in the whole oxide layer becomes homogeneous. Zirconium may migrate via NiAl grain boundaries, where it is known to segregate [15]. Thus, Zr present in the oxide can be expected to modify the stress relief by reducing the oxide creep rate. Zirconium delays the oxide scale spalling and inhibits the formation of cavities at the metal/oxide interface. And there is no voiding at the metal/oxide interface, unlike in Pt-modified NiAl coatings [14]. The absence of voiding in the presence of Zr is expected to improve alumina adhesion on the nickel aluminide.

The problem of designing the technology of coatings' deposition by CVD and PVD methods and designing the layers formed during aluminization remains open. The main difficulty is included in description of diffusion in a multi-component solid which leads to multi-phase formation.

In this work, the generalized Darken method is applied to calculate composition–distribution profiles for the elements present in the diffusion couple. The phase composition of the aluminized zone can be briefly predicted from the phase diagram, but the resulting morphology is described by the diffusion path. Hence, the diffusion path, which in the ternary phase diagram connects the terminal composition of the diffusion couple, can be calculated. When the isothermal section of the phase diagram is projected onto the composition triangle, then the fields crossed by the diffusion path can be indicated.

In this work the Ni-Al-Zr system is analyzed. The previous binary model [16, 17] is expanded and mass transport in the multicomponent system is taken into account, in which the layers of various phases and multiphase layers can grow.

***Corresponding author: Bartek Wierzba:** Research and Development Laboratory for Aerospace Materials, Faculty of Mechanical Engineering and Aeronautics, Rzeszow University of Technology, W. Pola 2, 35-959 Rzeszow, Poland. E-mail: bwierzba@prz.edu.pl
**Jolanta Romanowska, Maryana Zagula-Yavorska, Jan Sieniawski:** Research and Development Laboratory for Aerospace Materials, Faculty of Mechanical Engineering and Aeronautics, Rzeszow University of Technology, W. Pola 2, 35-959 Rzeszow, Poland
**Janusz Markowski:** Faculty of Electronics, Wroclaw University of Technology, Z. Janiszewskiego 11/17, 50-372 Wroclaw, Poland

The forthcoming sections of the paper are arranged as follows: the model of reactive diffusion in multicomponent and multiphase systems is formulated, the physical laws which constitute the theoretical framework are presented, then the experimental procedure is described and the results concerning reactive diffusion in an Ni-Al-Zr ternary system are presented. There are discussed two cases, for different Zr concentrations. The low zirconium concentration, when the amount of zirconium in smaller than the amount of aluminum and the high zirconium concentration, when amounts of zirconium and aluminum are equal, the initial zirconium and aluminum layers thickness are the same. The experimental results are compared with the data simulated by the presented method.

## 2 Physico-mathematical description

The interdifusson may be described by means of the generalized Darken or Onsager analysis [18, 19]. In this paper the Darken method is used for simulating multiphase Ni-Al-Zr system for the low zirconium content and the generalized Darken method [20–22] for the high zirconium content.

The core of the generalized Darken method is the mass conservation law:

$$\frac{\partial c_{i,j}}{\partial t}+\frac{\partial}{\partial \mathrm{x}}\left(c_{i,j}\upsilon_{i,j}^{d}+c_{i,j}\upsilon_{j}^{drift}\right)=0, \tag{1}$$

where $c_{i,j}$ denotes the concentration of the $i$-th component in the $j$-th phase; $\upsilon_{i,j}^{d}$ and $\upsilon_{j}^{drift}$ are the diffusion component velocity and the overall drift velocity in $j$-th phase, respectively.

In the presented analysis, a motion of a single phase $r$-component mixture, i.e., alloy or solid solution, is taken into account. The molar ratio, $N_{i,j}$, is defined as:

$$1:=\sum_i N_{i,j}:=\sum_i \frac{c_{i,j}}{c_j}$$

The mixture molar concentration in the $j$-th phase is a sum of the components molar concentrations and for simplification is accepted constant:

$$\sum_i c_{i,j}=c_j=const.$$

The component diffusion velocity, $\upsilon_{i,j}^{d}$, should be expressed by the proper constitutive formula. In this work the Nernst-Planck equation [23, 24] is implemented:

$$\upsilon_{i,j}^{d}=-B_{i,j}\frac{\partial \mu_{i,j}^{ch}}{\partial \mathrm{x}}, \tag{2}$$

where $\mu_{i,j}^{ch}$ is the chemical diffusion potential of the $i$-th component in the $j$-th phase; $B_{i,j}$ denotes the mobility.

The chemical potential can be expressed by the molar concentration as:

$$\mu_{i,j}^{ch}=\mu_{i,j}^{0}+RT\ln\left(c_{i,j}\gamma_{i,j}\right), \tag{3}$$

where $\mu_{i,j}^{0}$ denotes the standard, constant chemical potential of the $i$-th component and $\gamma_{i,j}$ its activity coefficient (further we assume that $\gamma_{i,j}\approx 1$). (4)

Finally, by coupling Eqs. (2) and (3) the diffusion velocity of the components can be expressed as:

$$\upsilon_{i,j}^{d}=-RTB_{i,j}\frac{\partial \ln c_{i,j}}{\partial \mathrm{x}}. \tag{5}$$

The drift velocity can be calculated from the mass conservation of the components, Eq. (1), with additional assumption of constant total molar concentration, thus:

$$0=\sum_i \frac{\partial c_{i,j}}{\partial t}=\sum_i \frac{\partial\left(c_{i,j}\upsilon_{i,j}^{d}+c_{i,j}\upsilon_{j}^{drift}\right)}{\partial x} \tag{6}$$

Finally, the drift velocity equals:

$$\upsilon_{j}^{drift}=-\sum_i \frac{c_{i,j}}{c_j}\upsilon_{i,j}^{d}. \tag{7}$$

To calculate the multiphase interdiffusion process additionally the reaction terms should be considered. In this paper two cases are considered: low and high zirconium content. When the zirconium content is low, it behaves as a marker in the NiAlZr system and therefore, the zirconium diffusion can be neglected during calculations (Fig. 5). When the zirconium content in the NiAlZr system is high, the diffusion of zirconium should be calculated (Fig. 6).

### 2.1 Low Zr content

In this case the reactive diffusion between the Ni and Al should be simulated. The generalized Darken method

should be supplemented with proper boundary conditions [25, 26]. The boundary conditions are used to calculate the concentrations of the components on each side of the phase boundary zone and to calculate the reaction rates of each phase. The boundary conditions follow the Leibnitz's rule:

$$\frac{\mathrm{d}}{\mathrm{d}t}\int_{a(t)}^{b(t)} f(x,t)\mathrm{d}x = \int_{a(t)}^{b(t)} \frac{\partial}{\partial t} f(x,t)\mathrm{d}x + \dot{b}(t) f(t,b) - \dot{a}(t) f(t,a). \quad (8)$$

The mass balance at the moving interfaces (left (L) and right (R) side of the phase) for each component follows Eq. (8), $f(t, x) = c_{i,j}$:

$$\left(c_{i,j+1}(R) - c_{i,j}(L)\right)\frac{\mathrm{d}X_j}{\mathrm{d}t} = J_{i,j+1}(R) - J_{i,j}(L), \quad (9)$$

for $i = 1,\ldots, r$, $j = 0,\ldots, n$. The $i$ and $j$ indexes denote the component and phase number, respectively. The $c_{i,j+1}(R) = c_{i,j+1}\left(X_j(t)\right)$ and $c_{i,j}(L) = c_{i,j}\left(X_j(t)\right)$ denotes the concentration of the $i$-component at the right side of the $j+1$ phase and the left side of the $j$ phase, respectively. The $J_{i,j+1} = c_{i,j+1}\upsilon^d_{i,j+1} + c_{i,j+1}\upsilon^{drift}_{j+1}$ is the overall flux of the $i$-th component in the $j+1$ phase. $X_j(t)$ is the boundary position, Fig. 1.

The $j$-phase volume follows Eq. (9), after summing over all components:

$$\frac{\mathrm{d}X_j}{\mathrm{d}t} = \sum_i \frac{\left(c_{i,j+1}\upsilon^d_{i,j+1} + c_{i,j+1}\upsilon^{drift}_{j+1}\right)(L) - \left(c_{i,j+1}\upsilon^d_{i,j+1} + c_{i,j+1}\upsilon^{drift}_{j+1}\right)(R)}{c_{i,j+1}(L) - c_{i,j+1}(R)} \quad (10)$$

for $j = 0,\ldots, n-1$.

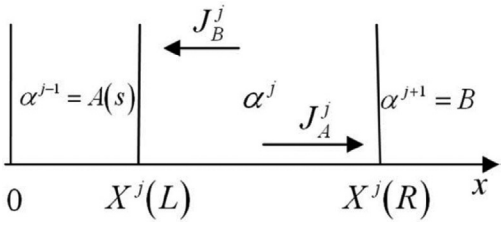


**Fig. 1:** The schematic presentation of the boundary conditions when low Zr content is simulated.

## 2.2 High Zr content

In this case the multiphase interdiffusion between all three components should be simulated, Fig. 6. The generalized Darken method should be implemented where the mass conservation is rewritten in average variables [27, 28]:

$$\frac{\partial \overline{c}_i}{\partial t} + \mathrm{div}\left(\overline{c}_i\overline{\upsilon}^d_i + \overline{c}_i\overline{\upsilon}^{drift}\right) = 0 \quad (11)$$

The average composition of the system in the spatial region is a weighted average of the compositions of the phases in the equilibrium, i.e. the compositions described by the tie-line ends, Fig. 2. The mass balance expressed for each component says:

$$\overline{c}_i = f_\alpha c_{i,\alpha} + (1 - f_\alpha)c_{i,\beta}, \quad i = 1, 2, 3. \quad (12)$$

In the one-phase region there is simply:

$$\overline{c}_i = c_{i,\alpha} \quad \text{or} \quad \overline{c}_i = c_{i,\beta} \quad (13)$$

depending on the phase.

The volume fraction, $f_j$, in a two-phase region, $c_{i,j}$ and $\upsilon_{i,j}$ are the concentration and overall velocity of the $i$-th component in $j$-th phase,

$$f_\alpha + f_\beta = 1, \quad 0 \le f_j \le 1. \quad (14)$$

Finally, the mass conservation in single $\alpha$ and $\beta$ phase regions can be rewritten in a form:

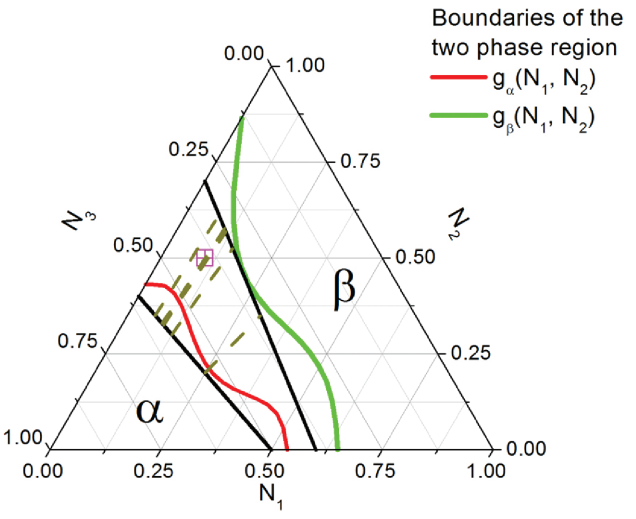


**Fig. 2:** The schematic presentation of the generalized Darken method.

$$\frac{\partial f_j c_{i,j}}{\partial t} + \mathrm{div}\left(f_j c_{i,j} \upsilon_{i,j}\right) = 0, \quad i = 1,2,3,\ j = \alpha, \beta \tag{15}$$

The overall average flux of the *i*-th component can be defined as:

$$\overline{c_i}\overline{\upsilon_i} = -f_\alpha D_{i,\alpha} \frac{\partial c_{i,\alpha}}{\partial x} - f_\beta D_{i,\beta} \frac{\partial c_{i,\beta}}{\partial x} + f_\alpha c_{i,\alpha} \upsilon_\alpha^{drift} + f_\beta c_{i,\beta} \upsilon_\beta^{drift}, \quad i = 1,2,3 \tag{16}$$

Figure 2 presents the schematic presentation of the proposed method – the interdiffusion of the three componet system between $\alpha$ and $\beta$ phases. On the composition triangle the phase boundaries are presented (functions $g_\alpha$ and $g_\beta$). Lines connecting boundaries show the tie-lines (conodes), which are the initial conditions from the phase diagram.

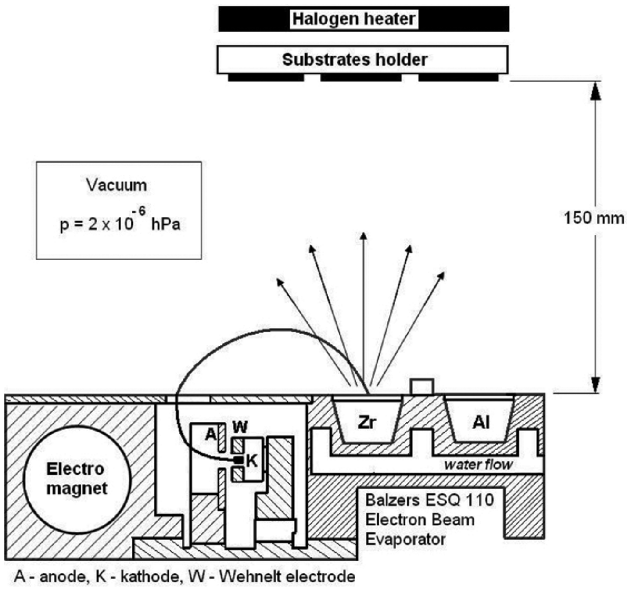


**Fig. 3:** Scheme of the apparatus of the EB-PVD method [37].

# 3 Experiments

The commercial nickel of 99.95 wt.% purity was used in this study. The cylindrical samples of the 20 mm diameter and 4 mm high were cut and grounded up to SiC No 1000, degreased in ethanol and ultrasonically cleaned.

Aluminum and zirconium thin layers (each 1 μm thick) or zirconium and aluminum layers (each 1 μm thick) were deposited by the EB-PVD method. In this method, the material to evaporate (placed in a water-cooled Cu crucible) is melted by focused high energy electron beam. Power density in electron beam spot (on the surface of the material) can reach over 40 kW/cm$^2$ and any material around the spot can be easily evaporated. Well-cooled walls of crucible protect the material against contamination by Cu. After the evaporation process, the material can be easily evacuated (it does not stick to the crucible). An additional advantage of this method is that material can have any form (wire, sheet pieces, pellets, etc.) and can be easily supplemented in the crucible. For this work, Balzers ESQ 110 (four hearts crucible) electron beam evaporator was used. Electrons emitted from a hot tungsten cathode (Fig. 3) are initially focused by the Wehnelt electrode and then are accelerated by the electric field to the anode and achieve energies up to 10 keV. Under the influence of the magnetic field, electron beam is focused and deflected (by an angle of 270°), forming a high energy electron spot on the surface of the material in the crucible. Due to four hearts crucible of ESQ 110, it is possible to obtain up to 4 different material layers on the substrate in one vacuum process.

All layers were deposited on motionless Ni substrates. The distance between the evaporating source (crucible) and substrates was 150 mm.

Technological stages for Al and Zr coatings deposition were as follows:

- substrates cleaning in a detergent and placing in a substrates holder
- pumping the chamber to $p = 2 \times 10^{-6}$ hPa
- substrate heating to 300 °C ($t_H = 20$ min)
- evaporation of the first layer (Zr or Al) with the rate (v) to obtain the proper coating thickness (evaporation time $t_E = 0.5$ min ÷ 7 min)
- crucible rotation (changing the position to another material)
- evaporation of the second coating (Zr or Al) with rate (v) to obtain the proper layer thickness (evaporation time $t_E = 0.5$ min ÷ 7 min)
- cooling substrates to 50 °C (about 1 hour)
- venting the chamber.

## 3.1 Low Zr content

The aluminide coatings were deposited on nickel with 1 μm thick aluminum and 1 μm thick zirconium layers (deposited by the EB-PVD method presented above) using the CVD equipment BPXPR0325S manufactured by IonBond Company (Fig. 4). The aluminizing process was performed for 8 h at the temperature 1325 K. After the aluminizing, the sample was annealed for 2 hours. Aluminum chloride vapor (AlCl3) was produced in an external generator I

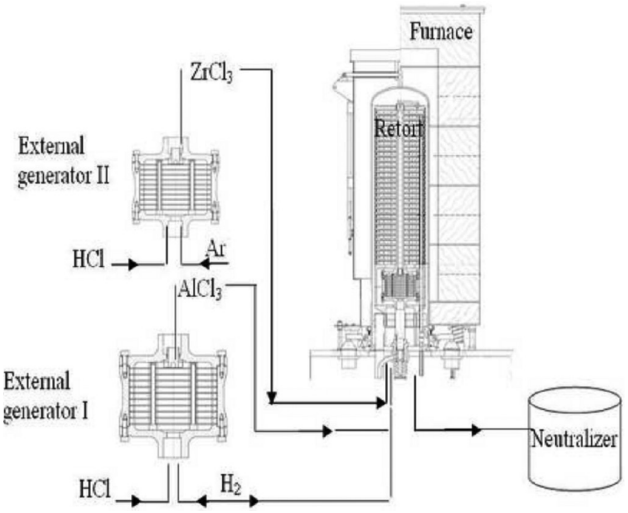


**Fig. 4:** The schematic presentation of the CVD equipment BPXPR0325S manufactured by IonBond Company [10].

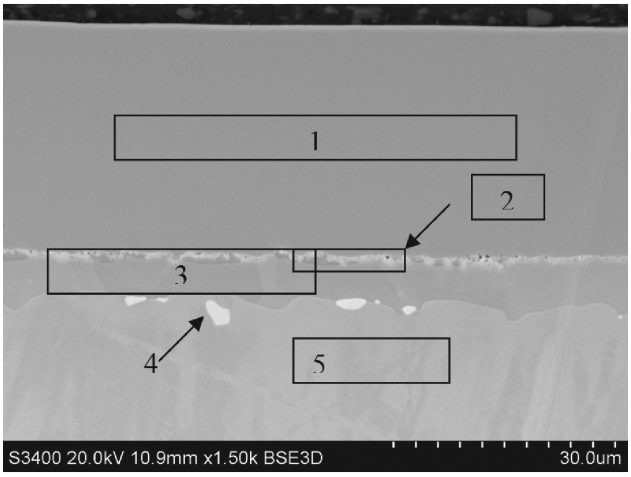


**Fig. 5:** Microstructure of the coating after the CVD aluminizing process after 8 h at 1325 K.

(Fig. 4), at 330 °C according to the reaction: $2Al + 6HCl \rightarrow 2AlCl_3 + 3H_2$. Then the saturating atmosphere was transported in a stream of hydrogen gas into the CVD reactor, where nickel samples were placed.

Zirconium chloride vapor ($ZrCl_3$) was produced in an external generator II at 440 °C according to the reaction: $2Zr + 6HCl \rightarrow 2ZrCl_3 + 3H_2$. The saturation atmosphere was transported in a stream of hydrogen gas into the CVD reactor, where nickel samples were placed.

In this case both zirconium and aluminum layers have the same thickness (1 μm) and additional aluminum is provided in the CVD process, so there is less zirconium than aluminum and this case is referred as the low Zr zirconium content. The microstructure of the cross-sections of the coating was investigated by scanning electron microscope (SEM) Hitachi S-3400N and energy dispersive spectroscope (EDS) (Fig. 5).

Figure 5 shows the microstructure on the cross-section of the Al/Zr coatings after 8 hours aluminizing process by the CVD method followed by 2 hours annealing. The coating consists of two zones: outer (about 30 μm thick) and inner zone (10 μm thick). In the outer zone the proportion of Ni, Al and Zr corresponds to the β-NiAl phase (Point 1 in Table 1). The chemical composition of the inner zone, distributed below the β-NiAl phase, corresponds to the $Ni_3Al$ phase (Point 3). Below the presence of pure nickel was detected (Point 5). Zirconium is situated in inclusions that are distributed at the phase boundaries between β-NiAl and $Ni_3Al$ (Point 2) and between $Ni_3Al$ and the nickel substrate (Point 4). It may be assumed that when the zirconium concentration is low it behaves as a marker.

**Table 1:** Chemical composition of the coatings after the CVD aluminizing process after 8 h at 1325 K.

| Point | Phase / Phase boundary | Chemical composition (at.%) | | |
|---|---|---|---|---|
| | | Al | Ni | Zr |
| 1 | β-NiAl | 39.88 | 60.05 | 0.07 |
| 2 | β-NiAl-$Ni_3Al$ | 20.06 | 59.94 | 20.00 |
| 3 | $Ni_3Al$ | 23.75 | 74.71 | 1.54 |
| 4 | $Ni_3Al$-Ni | 5.66 | 84.17 | 10.17 |
| 5 | Ni | – | 100 | – |

## 3.2 High Zr content

Zirconium layer (1 μm thick) and aluminum thin layer (1 μm thick) were deposited by the EB-PVD method (presented above) on the nickel samples. The samples with Zr and Al layers were subjected to diffusion treatment at 1325 K for 4 h in the argon atmosphere.

In this case, both zirconium and aluminum layers have the same thickness (1 μm), so it can be assumed that there is the same amount of zirconium and aluminum and this case is referred as high Zr content. The microstructure of the coating was examined by the use of an optical microscope Nikon Epiphot 300, a scanning electron microscope (SEM) Hitachi S-3400N and an energy dispersive spectroscope (EDS) (Fig. 6).

The coating consists two zones: outer (3–4 μm thick) zone and internal (6–7 μm thick) one. On the top of the coating the proportion of Ni, Al and Zr corresponded to γ-Ni(Al,Zr) phase (Point 1 in Table 2). The chemical composition of the inner zone, distributed below the Ni(Al,Zr) phase corresponds to the $Ni_5Zr$ phase (Point 2).

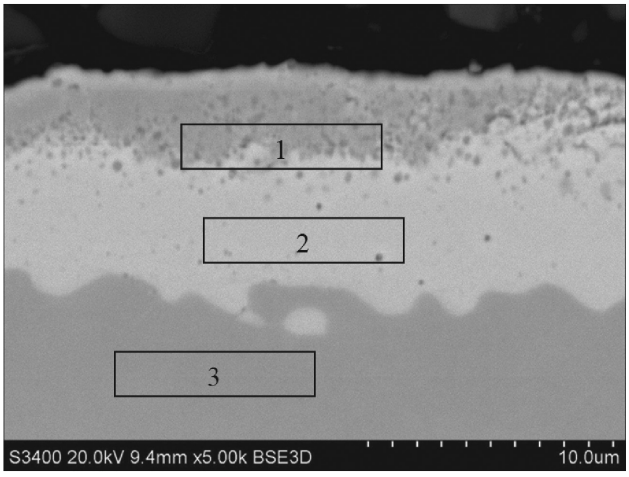


**Fig. 6:** Microstructure of the coating deposited by EB-PVD method after diffusion treatment after 4 h at 1325 K.

**Table 2:** Chemical composition of the coating deposited by EB-PVD method after diffusion treatment process after 4 h at 1325 K.

| Point | Phase / Phase boundary | Chemical composition (at.%) | | |
|---|---|---|---|---|
| | | Al | Ni | Zr |
| 1 | γ-Ni(Al,Zr) | 7.57 | 86.20 | 6.23 |
| 2 | $Ni_5Zr$ | – | 82.66 | 17.34 |
| 3 | γ-Ni(Al,Zr) | 2.91 | 95.48 | 1.61 |

Below the presence of the γ-Ni(Al,Zr) phase was detected (Point 3).

# 4 Results

## 4.1 Low Zr content

According to Campbell [29], Ma, Ardell [30] and Wei et al. [31], it has been assumed that the interdiffusion coefficient in the NiAl (beta) phase depends on the concentration. In this work the integral interdiffusion coefficient $\tilde{D}^{Int}_{NiAl}$ in NiAl phase from Campbell approximation [29] was applied. The Ni-Al binary system [32, 33] has several intermetallic phases. Two of them (AlNi and $AlNi_3$) were considered. The data used in simulations are shown in Table 3 [34–36].

Figure 7 presents the spatial distribution of the concentration profile. The presented data describe the changes of the composition of the system. Two phases, $AlNi_3$ and AlNi are formed. Zirconium is only on phase boundaries, which indicates that it behaves as a marker.

**Table 3:** Thermodynamic and kinetic data used to simulate the reactions in the Ni-Al system at 1323 K.

| Phase, j | Range of $N_{Ni}$ | Diffusion coefficient, $D^j_{Ni,Al}$ ($cm^2s^{-1}$) |
|---|---|---|
| Ni | 1–0.85 | $4.24 \times 10^{-12}$ |
| $AlNi_3$ | 0.77–0.725 | $2.92 \times 10^{-11}$ |
| AlNi | 0.625–0.45 | $1.55 \times 10^{-10}$ |
| Al | 0 | $2.15 \times 10^{-11}$ |

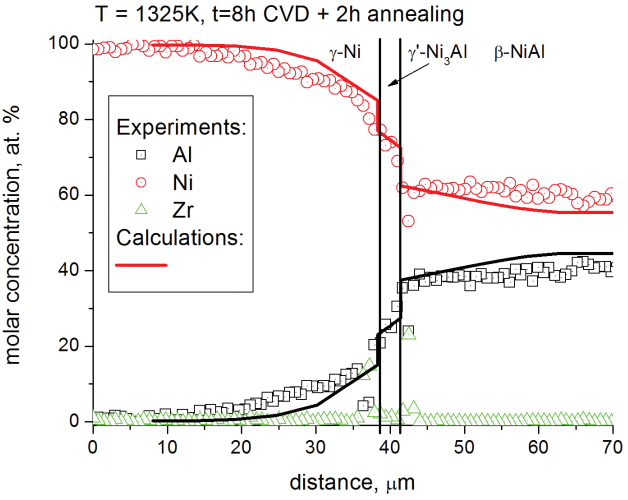


**Fig. 7:** The comparison of the concentration profile of the NiAl multiphase diffusion experiments (dots) and simulations (line).

## 4.2 High Zr content

When zirconium content is high the diffusion coefficients in γ-Ni phase based is on Campbell approximation [29]. The diffusion between γ-Ni and $Ni_5Zr$ phase is analyzed. The Zr diffusion coefficient is approximated basing on the Grandjean and Limoge data [37], Table 4.

The phase boundaries presented in Figure 9 are described by the polynomial functions, $f\left(\gamma \,|\, \gamma + Ni_5Zr\right) = 0.225 - 15N_{Zr}$ and $f\left(\gamma + Ni_5Zr \,|\, Ni_5Zr\right) = -0.005 + 0.125N_{Zr}$. The initial concentrations of the components are presented in Table 4. The set of the equations shown in section 2.2. High Zr content was used to calculate the diffusion in Ni-Al-Zr system.

Figures 8 and 9 present the spatial distribution of the concentration and the diffusion path respectively. The presented data describe changes of the average composition of the system parallel to the mass transport direction, as it results from the concentration profiles. It is seen that the diffusion path passes the γ-Ni + $Ni_5Zr$ two-phase region. The points where the diffusion path crosses the interphase boundaries determine the average compositions

**Table 4:** Thermodynamic and kinetic data used to simulate the reactions in Ni-Al-Zr system at 1325 K.

| Phase, j | Al diffusion coefficient, $D_{Al,j}$ ($cm^2s^{-1}$) | Ni diffusion coefficient, $D_{Ni,j}$ ($cm^2s^{-1}$) | Zr diffusion coefficient, $D_{Zr,j}$ ($cm^2s^{-1}$) |
|---|---|---|---|
| γ-Ni | $4.24 \times 10^{-12}$ | $4.24 \times 10^{-12}$ | $10^{-15}$ |
| $ZrNi_5$ | $4.24 \times 10^{-12}$ | $4.24 \times 10^{-12}$ | $10^{-15}$ |
| **Initial concentration (at.%)** | | | |
| γ-Ni | 0 | 100 | 0 |
| $ZrNi_5$ | 5 | 80 | 15 |

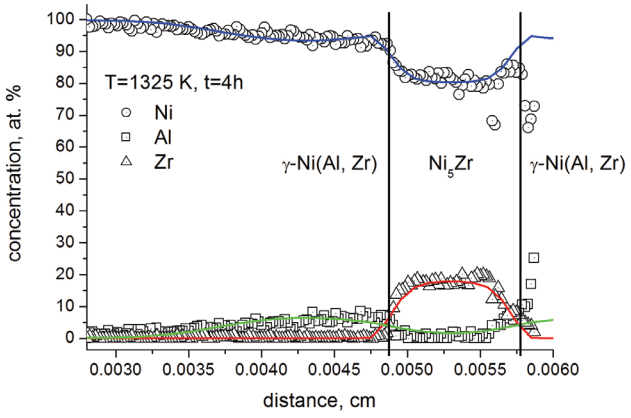


**Fig. 8:** The comparison of the concentration profile of the NiAlZr multiphase diffusion experiments (dots) and simulations (line).

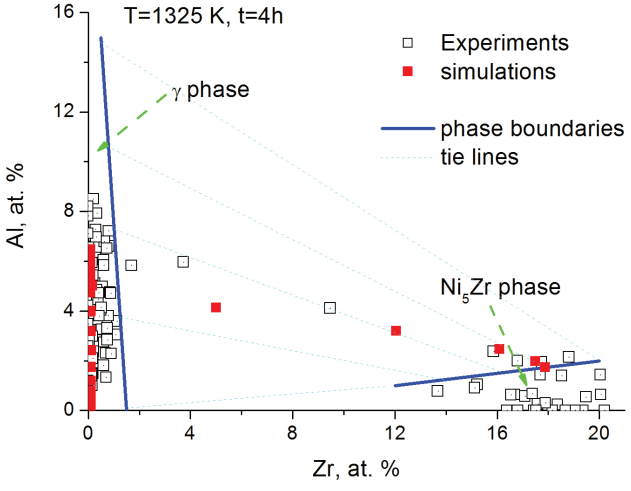


**Fig. 9:** The part of the Ni-Al-Zr phase diagram [38] at 1325 K. Two phases can be distinguished: γ-Ni and $Ni_5Zr$ phase. The comparison of the experimental (empty dots) and computational (full dots) diffusion paths.

of the system for which any phase (dis)appears or one phase transforms into the other.

# 5 Conclusion

The addition of small amounts of reactive elements such as Zr, Hf, Y, or Ce to the β-NiAl coatings has beneficial effects on the oxidation behavior. The beneficial effects include improvement in adhesion of alumina scales and reduction of oxide scale growth rate. Zirconium co-deposited with aluminum on the nickel superalloy by the CVD process was discussed in this paper. The model of reactive diffusion in two- and three-component systems was proposed by means of the generalized Darken method with proper boundary conditions. The model includes both drift and diffusion velocities. It was shown that the low content of zirconium do not influence calculations. It was presented that in this case Zr behaves as a marker. When the Zr content is high, the model should include all three components diffusion.

**Funding:** This work has been supported by the National Science Centre (NCN) in Poland, decision number 2011/01/B/ST8/05036.

# References

[1] F.A. Khalid, N. Hussian, A.H. Qureshi, *Mat. Eng. Perf.* 11 (2002) 211.
[2] E. Gariboldi, M. Verani, Ch. Riva, *Advanced Mat. Res.* 278 (2011) 228.
[3] R. Rajendran, M. Ganeshachar, Jivankumar, T. Rao, *Eng. Fail. Anal.* 18 (2011) 2104.
[4] A. Nowotnik, J. Sieniawski, M. Góral, M. Pytel, K. Dychtoń, *Arch. of Mat. Sci. and Eng.* 55 (2012) 22.
[5] P. Visuttipitukul, N. Limvanutpong, P. Wangyao, *Mat. Trans.* 51 (2010) 982.
[6] A. Smith, A. Kempster, J. Smith, *Surf. and Coat. Techn.* 120–121 (1999) 111.
[7] M. Zielińska, M. Zagula-Yavorska, J. Sieniawski, R. Filip, *Arch. of Metal. and Mat.* 58 (2013) 697.
[8] M. Yavorska, J. Sieniawski, M. Zielińska, *Arch. of Metal. and Mat.* 56 (2011) 187.
[9] M. Zielińska, J. Sieniawski, M. Yavorska, M. Motyka, *Arch. of Metal. and Mat.* 56 (2011) 193.
[10] M. Zagula-Yavorska, J. Sieniawski, T. Gancarczyk, *Arch. of Metal. and Mat.* 57 (2012) 503.
[11] J. Romanowska, *CALPHAD* 44 (2014) 114.
[12] B. Pint, T. Haynes, T. Besmann, *Surf. and Coat. Techn.* 205 (2010) 3287.
[13] Y. Wang, M. Suneson, G. Sayre, *Surf. and Coat. Techn.* 206 (2011) 1218.

[14] S. Hamadi, M. Bacos, M. Poulain, A. Seyeux, V. Maurice, P. Marcus, *Surf. and Coat. Techn.* 204 (2009) 756.
[15] D. Larson, M. Miller, *Mater. Charact.* 44 (2000) 159.
[16] M. Danielewski, B. Wierzba, A. Gusak, M. Pawełkiewicz, J. Janczak-Rusch, *J. App. Phys.* 110 (2011) 123705.
[17] B. Wierzba, M. Danielewski, K. Tkacz-Śmiech, J. Sieniawski, *CVD* 18 (2012) 267.
[18] M. Danielewski, B. Wierzba, *MMTB* 39B (2008) 629.
[19] M. Danielewski, B. Wierzba, *Acta Mat.* 58 (2010) 6717.
[20] W.D. Hopfe, J. Morral, *Acta Metall. Mater.* 42 (1994) 3887.
[21] M. Danielewski, B. Wierzba, K. Tkacz-Smiech, A. Nowotnik, *Comp. Mat. Sci.* 69 (2013) 1.
[22] B. Wierzba, M. Danielewski, *Phil. Mag.* 91 (2011) 3228.
[23] W. Nernst, *Z. Phys. Chem.* 4 (1889) 129.
[24] M. Planck, *Annu. Rev. Phys. Chem.* 40 (1890) 561.
[25] M. Danielewski, B. Wierzba, A. Gusak, M. Pawełkiewicz, J. Janczak-Rusch, *J. Applied Phys.* 110 (2011) 123705.
[26] B. Wierzba, M. Danielewski, K. Tkacz-Śmiech, J. Sieniawski, *CVD* 18 (2012) 267.
[27] B. Wierzba, K. Tkacz-Śmiech, *Phys. A* 392 (2013) 1100.
[28] B. Wierzba, K. Tkacz-Śmiech, A. Nowotnik, *CVD* 19 (2013) 267.
[29] C. E. Campbell, *Acta Mat.* 56 (2008) 4277.
[30] Y. Ma, A.J. Ardell, *Mat. Sci. & Eng. A* 516 (2008) 259.
[31] H. Wei, X. Sun, Q. Zheng, G. Hou, H. Guan and Z. Hu, *J. Mater. Sci. Technol.* 20 (2004) 196.
[32] I. Ansara, N. Dupin, H.L. Lukas and B. Sundman, *J. of Alloys and Comp.* 247 (1997) 20.
[33] FactSage metal alloy databases, www.csct.polymtl.ca
[34] R.E. Hoffman, F.W. Pikus, R.A. Ward, *Trans. AIME* 206 (1956) 483.
[35] T.S. Lundy, J.F. Murdock, *J. Appl. Phys.* 33 (1962) 1671.
[36] J.R. MacEwan, J.U. MacEwan, L. Yaffe, *Can. J. Chem.* 37 (1959) 1623.
[37] A. Grandjean, Y. Limoge, *Acta Mater.* 45 (1997) 1585.
[38] FactSage software, www.factsage.com